Article

Electron Tunneling at Electrocatalytic Interfaces

Mohammad R. Nouri, Regina M. Kluge, Richard W. Haid, Jill Fortmann, Alfred Ludwig, Aliaksandr S. Bandarenka,* and Vitaly Alexandrov*

Read Online

ACCESS | Metrics & More | Article Recommendations | Supporting Information

ABSTRACT: It was recently proposed that tunneling current fluctuations in electrochemical scanning tunneling microscopy (EC-STM) can be used to map the electrocatalytic activity of surfaces with high spatial resolution. However, the relation between the increased noise in the electron tunneling signal and the local reactivity for such complex electrode/electrolyte interfaces is only explained qualitatively or hypothetically. Herein, we employ electron transport calculations to examine tunneling at Pt surfaces under the conditions of the oxygen reduction reaction as a case study. By computing current−voltage characteristics, we reveal that the tunneling barrier strongly depends on the chemical identity of the adsorbed reaction intermediate as well as on the orientation of the average dipole moment of water species mediating electron tunneling. Our theoretical results combined with EC-STM measurements suggest that detecting reaction intermediates at electrified interfaces in *operando* conditions is possible based on tunneling noise amplitudes. This study also aims to stimulate further explorations of tunneling-based electron-proton transfers to enable quantum electrocatalysis beyond conventional approaches.
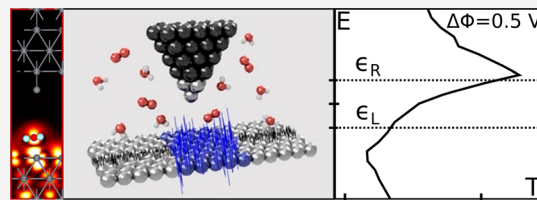
1. INTRODUCTION

Electron transfer (ET) is one of the most fundamental processes in nature underlying all redox reactions. The pioneering works of Rudolph Marcus, starting in 1956, have laid out a general theoretical framework enabling the analysis of ET in a broad spectrum of phenomena.[1−3] The Marcus theory allows one to evaluate the rates of ET reactions considering electron jumping between redox centers over the activation barrier. The required energy is provided by thermally induced reorganization of the solvent. However, it is established that ET may also occur via a completely quantum-mechanical mechanism avoiding ET over the potential barrier but instead cutting through the barrier. The concept of quantum electron tunneling (the term is used interchangeably with "electron tunneling") was introduced in the theoretical treatments of Hund,[4] Nordheim,[5] and others right after quantum mechanics was born. In 1928, George Gamow exploited tunneling to theoretically explain radioactive decay.[6] Since then, the theory of quantum-mechanical tunneling has been extended to an even wider range of physical phenomena and chemical species. As a matter of fact, at least five Nobel prizes in physics were awarded for research involving tunneling as an essential physical mechanism.[7]

Nowadays, electron tunneling plays a key role in nanotechnology. For example, it is the basic working principle of scanning tunneling microscopy (STM).[8,9] Solid-state tunnel junctions have become an active area of research in electronics and spintronics.[10−15] In biology, the structures of proteins and DNA were also shown to substantially accelerate electron transport by lowering tunneling barriers to achieve physiologically significant values.[16−18] Most prior investigations,

however, have been performed with systems either under ultra-high vacuum (UHV) conditions or involving dielectric solid thin films between metal electrodes. Studies probing electron tunneling at metal/liquid interfaces are also available, but interpretation of these measurements is highly challenging due to the greater complexity of the dynamic solution media.

Interfacial ET obviously plays a central role in electrocatalysis. Until quite recently, electron tunneling has been primarily considered as irrelevant "noise" accompanying a faradaic current associated with a local reaction. Yet, the importance of electron tunneling for electrochemical reactions at metal electrodes was recognized as early as 1931 by Gurney.[19] Later, the idea of studying interfacial redox reactions using tunneling was developed in the theoretical works of Kuznetsov, Ulstrup, Nitzan, and others.[20−25] Compared with vacuum, the measured tunneling barriers in solution-filled metal junctions are significantly reduced (from 4−5 down to 1−2 eV).[26,27] According to prior theoretical investigations, enhanced electron tunneling at metal/liquid interfaces is due to solvent structuring at the interface enabling efficient tunneling via H-bonding networks.[22,24,25] However, how exactly the molecular structure and composition at such interfaces promote or hinder tunneling remains poorly understood.
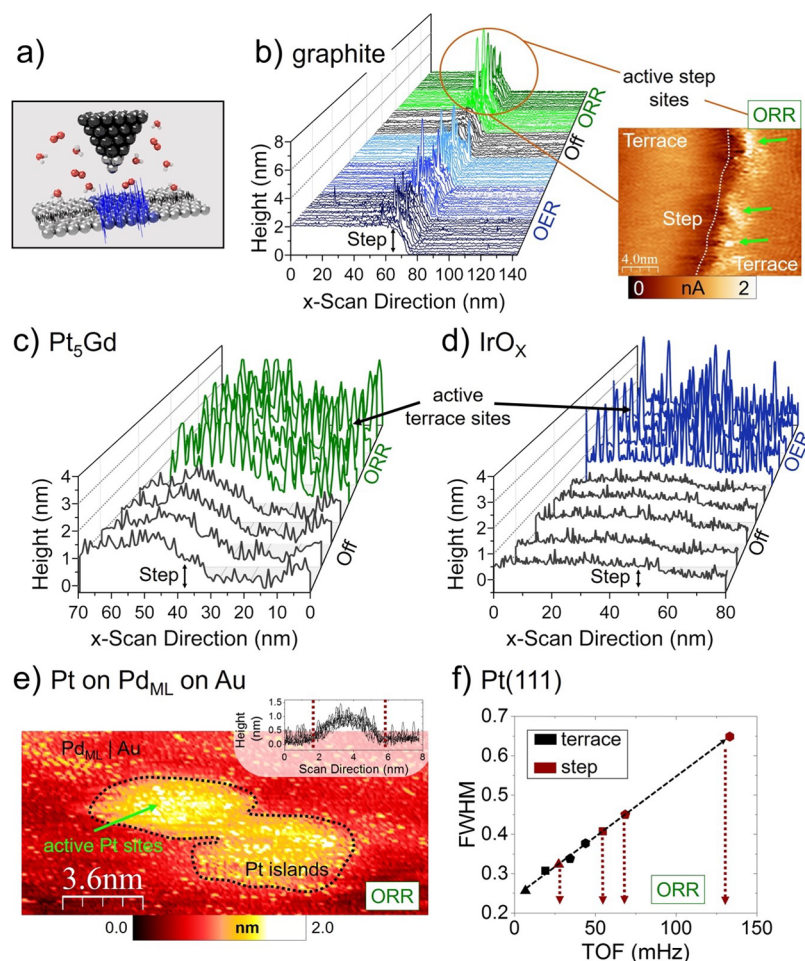
Figure 1. (a) Sketch of the working principle of EC-STM for detecting an enhanced local activity (blue atoms) by a higher noise level of the signal. (b) On a carbon-based electrode, both the active sites for OER (blue line scans) and ORR (green line scans) are located at step edges. Zoomed-in is an example of an EC-STM measurement providing atomic resolution of a step edge. Under ORR conditions, single active sites can be distinguished near the step sites (marked with green arrows). Data published in ref 38. (c, d) On transition metal catalysts, terrace sites show profound activity, marked with arrows: (c) polycrystalline Pt_5Gd for the ORR (green line scans, left)[39] and (d) amorphous IrO_x for the OER (blue line scans, right).[34] For comparison, the gray data show the surface when neither reaction takes place. (e) To investigate multiple catalyst materials on the same sample, Pt islands were deposited on a Pd monolayer on an Au substrate (see main text and SI for more information). The inset shows the scan over the Pt island. With high resolution, active Pt islands can be detected for the ORR, showing no edge effects. (f) Semiquantitative approach was conducted on Pt(111) model surfaces for the ORR, giving a direct relation between the noise level of the signal (FWHM, see text for more details) and the local TOF of terrace and step sites. See ref 33 for more details.

Interestingly, recent experimental studies have suggested that tunneling-barrier fluctuations manifested as noise features in the electrochemical STM (EC-STM) data could be used to characterize catalytically active surface sites under reaction conditions.[28,29] It has been demonstrated in the example of the hydrogen evolution reaction (HER)[30,31] and oxygen reduction reaction (ORR) at a Pt-based electrode[32] that the local noise signals can be exploited to quantify the local catalytic activity by correlating tunneling noise amplitudes with turnover frequencies (TOFs).[33] Recently, the applicability of this technique was extended to the oxygen evolution reaction (OER) on metal-oxide catalysts.[34] These experimental results suggest that not only do the changes in the water structure at the interface affect the tunneling probability but also the nature of the reaction intermediates. Ideally, such measurements combined with correct theoretical interpretations can endow the EC-STM technique with the capability of distinguishing reacting species at electrocatalytic interfaces.

In this work, we first discuss experimental results on the tunneling behavior of electrode/STM-tip junctions focusing on ORR/OER processes. Then, we present the results of our electron tunneling calculations aimed at elucidating the origin of the reaction-triggered noise phenomena in the STM measurements. For our theoretical analysis, we choose the ORR process considering the corresponding reaction intermediates adsorbed on two representative Pt facets, (111) and (110), as theoretical models.

2. METHODOLOGY

The ability to use fluctuations in the STM signal to locally identify active areas under reaction conditions was first published in ref 27 and further developed to be applicable to the HER, ORR, and OER processes.[29−34] This demonstrates the generality of the observed tunneling phenomenon across many electrocatalytic interfaces. These studies are in general agreement with other STM experiments on a variety of electrode/electrolyte systems that provided insights into the

reactivity of adsorbed adlayers[35] and single-molecule adsorbates.[36] The overall experimental approach is based on the observation of an increase in the noise level in the STM signal if the tip is positioned over an active area, as sketched in Figure 1a. A more detailed description of the experimental technique, along with further experimental details, is provided in SI.

Figure 2 shows the overall scheme of a two-electrode device configuration that mimics the experimental electrode/electro-
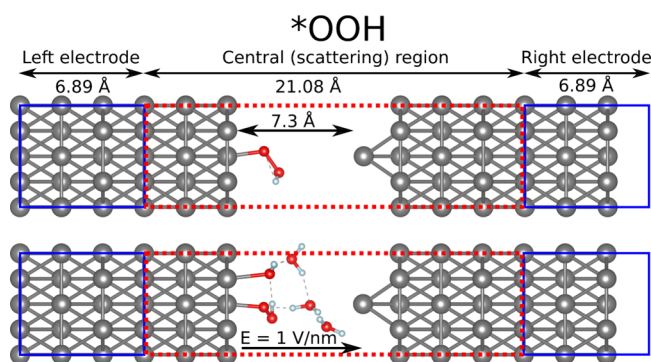
Figure 2. Schematic showing the junction comprised of two Pt electrodes and the scattering region used in electron tunneling calculations with the corresponding dimensions. The STM tip is modeled as the Pt(111) surface with a Pt adatom. In the figure, two scenarios are shown in the example of the *OOH intermediate: when the ORR intermediate adsorbed on Pt(111) is considered without (top panel) and with (bottom panel) surrounding water molecules. The atomic configurations for electron tunneling calculations are obtained through structural optimization of the scattering region under the applied uniform electric field as described in SI.

lyte/STM-tip setup used in our simulations. This configuration consists of the central scattering region sandwiched between two Pt electrodes serving as the source and the drain. The gap between the Pt electrode and the STM tip (modeled as the Pt(111) surface with a Pt adatom) was chosen to be consistent with experiments which are typically within the 0.5−1 nm range. We consider two models of the Pt/electrolyte interface: (1) the surface with an adsorbed ORR intermediate, and (2) the surface with an adsorbed ORR intermediate plus four H_2O molecules corresponding to ~1 g/cm^3 water density to simulate the local water environment. The geometries with additional H_2Os in the gap region are first optimized in a uniform electric field with the strength of 1 V/nm approximating the applied bias between the electrode and the STM-tip in experiments. These optimized structures are then used in electron transport calculations with QuantumATK.[37] All further computational details, including the relevant convergence tests, are provided in SI.

3. RESULTS AND DISCUSSION

In the past, various electrocatalytic systems have been tested under the presence of oxygenated species in the tunneling gap, some of which are shown in Figure 1. Graphite is often used either as the support material or as the basis for low-cost catalysts for ORR and OER processes. As can be seen in Figure 1b for the graphite electrode, only step sites are active toward both oxygen reactions. Benefiting from the high-resolution capabilities of the STM technique, an atomically resolved image of a step edge is also shown in the inset. The active step sites can be recognized as the spots of high tunneling intensity colored in white in the image and pointed by green arrows.

More experimental details about the carbon system are reported in ref 38.

Moving on to the state-of-the-art catalysts, Figure 1c,d shows the experimental results for polycrystalline Pt$_5$Gd (ref 39) and amorphous iridium oxide IrO$_x$ (ref 34) tested under ORR and OER conditions, respectively. For both systems, a pronounced increase in the noise level across terrace sites can be found, being in line with the superior macroscopic activity assigned to those transition metal (oxide) surfaces.

Figure 1e shows the data of EC-STM measurements across Pt islands deposited on a Pd monolayer on an Au substrate. This research was motivated by the approach of "high-entropy alloys" that were reported to show great promise as ORR catalysts.[40−42] Under ORR conditions, especially the interior of the Pt islands exhibits the highest noise level and thus activity. The Pd monolayer shows some minor activity without the detection of any pronounced activity of the edge between Pt and Pd. On the other hand, the Au substrate remains inactive toward the ORR, as shown in Figure S2. Notably, no pronounced activity at the transition between the Pt−Pd and Pt−Au phases was detected. With this strategy, it becomes possible to further elucidate catalytic materials consisting of multiple metals, including edge effects at boundaries between two or more materials.

These examples of very different catalyst materials clearly demonstrate that the enhanced noise level of the STM signal in localized regions is directly associated with electrocatalytic activity. To elaborate on this noise-activity relation further, we employed a semiquantitative approach considering the ORR process for the Pt(111) model system.[33] In general, to obtain a quantitative measure for the noise level of a certain STM signal, we consider the derivative of the STM signal with respect to adjacent data points. In the case of data recorded in the constant-current mode as shown in Figure 1 (except the inset of b), it would be the "height" (tip-sample distance) derived with respect to the scan direction ($\partial z/\partial x$). Histograms are then compiled from those signal derivatives and analyzed with a Gaussian fit. The full-width-at-half-maximum (FWHM) of the Gaussian fit is then employed as the noise level of a signal: The more noise in the signal, the more pronounced the deviations of the signal derivatives, and the higher the FWHM. More information on this quantification approach is given in ref 33., and Chapter 1.4 of the SI. For the Pt(111) model study for the ORR, the outcome of this analysis is provided in Figure 1f: a linear trend is obtained between the measure for the noise level of the given data set (FWHM) and the TOF of the terrace sites. Guided by this linear relation, we could extrapolate a local TOF of adjacent step sites. By doing so, we were not only able to quantitatively confirm a direct relationship between noise level and activity but could also use this relation to extract an activity level for step sites. This trend has recently been empirically confirmed by Granozzi et al.[29,31]

As a side note, the here reported EC-STM measurements can be conducted both in constant current and constant height mode. Analog, the constant height mode, can be used to record an image, in which the active sites can be identified by their higher noise level. An example is given in the inset of Figure 1b. Similarly, for the quantification approach, the signal derivative (here tunneling current versus time) can be employed. Also here the FWHM is directly related to activity, as discussed in ref 33.

Thus, we can empirically prove that there is a direct relationship between the observed noise features in the EC-
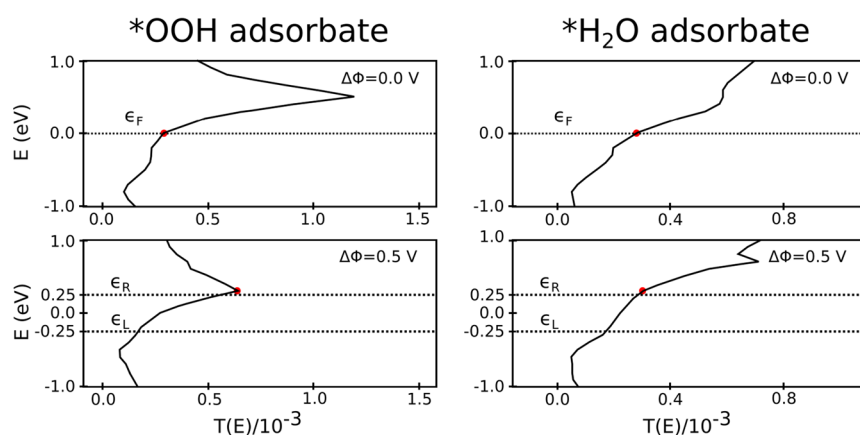
Figure 3. Calculated k-point averaged electronic transmission spectra as a function of energy for the *OOH and *H_2O adsorbates in the junction (see Figure 2). The results of zero-bias calculations ($\Delta\Phi = 0$ V) are shown in the top portion, whereas finite-bias ($\Delta\Phi = 0.5$ V) calculations are illustrated in the bottom portion of this figure. The dotted lines indicate the Fermi energy (ε_F) at $\Delta\Phi = 0$ V, and the Fermi levels of the left (ε_L) and right (ε_R) electrodes separated by the bias of $\Delta\Phi = 0.5$ V. The transmission at the Fermi energy for zero-bias and the maximum transmission between μ_L and μ_R for finite-bias calculations are depicted by red points.

STM signal and a local increase in the ORR/OER activity. We can therefore assume, based on the behavior of ORR and OER catalysts, that there may be a dependence on the nature of the reaction intermediates. However, the question remains whether electrochemical STM experiments are capable of distinguishing surface-bound reaction intermediates for the liquid-filled junctions. Therefore, we next commence explicit electron tunneling calculations to elucidate the origin of the noise level−activity relation, which was only demonstrated empirically so far.

We first discuss our electron tunneling results obtained for the simplest model involving only adsorption intermediates in the junction in the absence of water molecules (see the top panel in Figure 2). Figure 3 shows the electronic transmission spectra as a function of energy for the adsorbed OOH and H_2O intermediates from zero- and finite-bias calculations. Similar plots for the flat surface models of the Pt(111) and Pt(110) facets along with the contour plot of the transmission coefficients vs reciprocal vectors k_A and k_B are provided in SI (Figure S6). The obtained results demonstrate that the changes in the transmission spectrum are more significant for adsorbed OOH upon application of external bias.

Figure 4 shows the cut-plane representations of transmission eigenstates for the ORR intermediates at the finite bias. The plots clearly show the involvement of adsorbed reaction intermediates and Pt atoms of the electrodes (especially from the topmost layer) in electron transmission across the junction. The largest participation can be observed in the case of *OOH adsorbate. We note that qualitatively similar results are obtained for the Pt(111) and Pt(110) surfaces with a flat tip (see Figure S7). We also point out that the electron tunneling characteristics are much less modified when going from zero to finite bias for the *O intermediate as compared to *OOH. This could be the explanation for why the noise measurements for the OER on metal oxide surfaces, which often show relatively low intrinsic electron conductivity, were still successful.[34]

To demonstrate even further how electron tunneling depends on external bias in simulations, we compare the computed current−voltage ($I-V$) characteristics for all ORR adsorbates. Figure 5 shows the obtained $I-V$ relations for different ORR intermediates at the Pt(111) surface for single
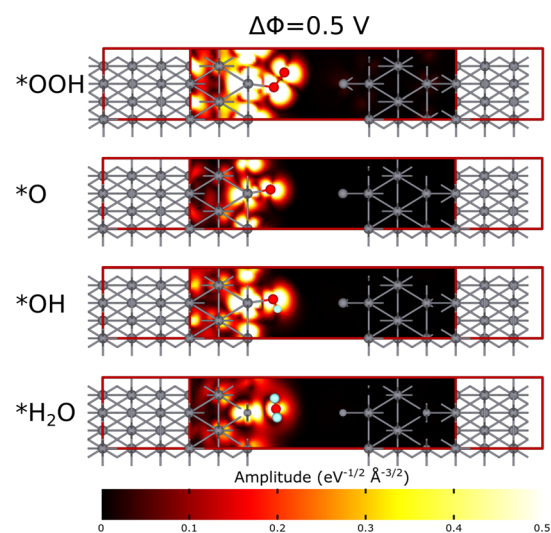
Figure 4. Cut-plane representation of electron transmission eigenstates for the O, OH, H_2O, and OOH species adsorbed on the Pt(111) surface as obtained from electron tunneling calculations at the bias of $\Delta\Phi = 0.5$ V (see the red points in Figure 3). To show which eigenstates contribute more to the electron tunneling, the cut-planes are chosen to be along the YZ plane in a way to show the highest contributing eigenstates. Note that each presented cut-plane corresponds to specific values of three parameters: energy, set of k-points (k_A, k_B), and the transmission eigenstate belonging to the same set of k-points. For each set of k-points, there might be more than one eigenstate (channel) contributing to the electron tunneling. Here, the largest one is selected to best demonstrate the difference between various reaction intermediates.

adsorbates (corresponding to the top panel of Figure 2) and in the presence of water environment (see the bottom panel of Figure 2). The results for a flat tip are provided in SI and are qualitatively similar (see, e.g., Figure S8). The potential region is chosen based on previous experimental data for the ORR over Pt electrodes.[27,28] The main observation is that the tunneling currents at 0.5 V for the OOH systems are significantly larger than the values obtained for other species. For example, for *OOH surrounded by H_2Os the current of ~1.2 μA is around three times larger than the one estimated for adsorbed H_2O. We also note that the absolute values of the
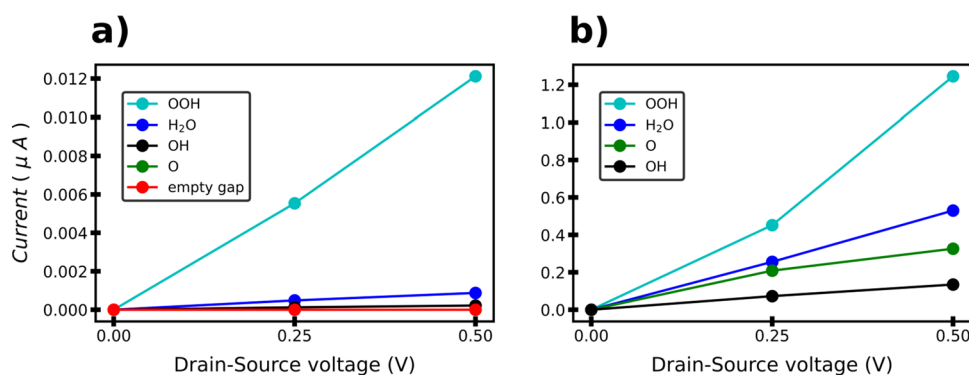
Figure 5. Computed tunneling current−voltage ($I-V$) characteristics of the Pt(111) surface with isolated absorbed ORR intermediates (a) and for the same ORR intermediates in the presence of water molecules (b).

tunneling current seem to be reasonable for the given size of the gap (7.3 Å), applied voltage (up to 0.5 V)[22] and being higher in the presence of solution H_2Os mediating electron tunneling.

It is established that the measured tunneling current is sensitive to the water structure at metal/water interfaces,[22] while our present simulations correspond to static water configurations. Therefore, to gain insights into how fluctuations of the average dipole moment of water media between the STM tip and the electrode surface may affect tunneling probabilities, we next analyze how rotations of an H_2O molecule could modify the amplitude of the tunneling current. To simplify this analysis, we consider the structural model with one H_2O placed in the middle of the junction, as shown in Figure 6. This allows us to single out the effect of the water
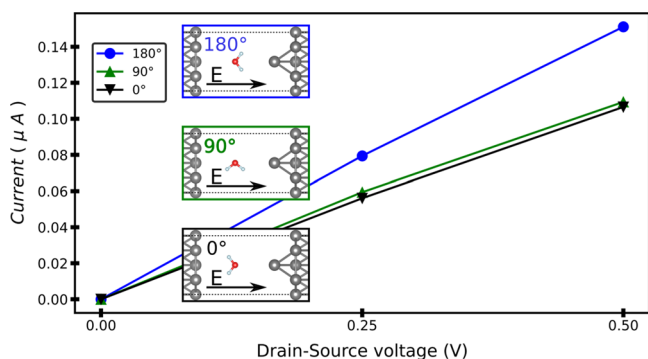
Figure 6. Tunneling current as a function of H_2O's dipole electric moment as H_2O rotates about the X-axis. H_2O is placed in the middle of the gap.

dipole orientation. As seen from the figure, when the direction of the dipole moment is along the electric field (180° rotation), the tunneling current is higher. On the other hand, when the electric field is screened by the dipole moment (no rotation), the tunneling current is decreased. Qualitatively similar results are obtained for the adsorbed H_2O molecule on both the Pt(111) and Pt(110) facets with the flat Pt tip (see Figure S8). These results show that water species mediating electron tunneling between the electrode and the STM tip will dynamically modulate the width of the tunneling barrier.

4. CONCLUSIONS

In summary, we have performed a theoretical analysis of electron tunneling at two Pt surfaces, (111) and (110), in the

presence of the ORR intermediates motivated by the observation of tunneling-noise features in the EC-STM signal across multiple water-splitting electrocatalysts. Our modeling results reveal the possibility of resolving different active sites at electrocatalytic interfaces based on the tunneling noise amplitudes, thus supporting experimental investigations. Further detailed studies are necessary to deepen our fundamental understanding of how tunneling probabilities depend on different factors such as the nature of the electrode and electrocatalytic reaction and electrolyte composition. This can enable quantitative interpretation of the EC-STM data to directly identify catalytically active sites with atomic resolution in situ. We also note that with a better understanding, tunneling control of chemical reactivity could become a key mechanistic principle in chemical kinetics, next to thermodynamic and kinetic control. This could potentially bring important advances to the issue of chemical selectivity since electron tunneling is possible even for reactions with high activation barriers. Our present theoretical study is a step in this direction. We also envision that a basic understanding of coupled electron and proton tunneling at electrochemical interfaces can, in the future, pave the way toward quantum electrocatalysis. This may help to circumvent some limitations of conventional approaches in electrocatalysis. In this regard, future theoretical investigations should also incorporate proton tunneling at electrocatalytic interfaces and how it couples with electron tunneling.

■ ASSOCIATED CONTENT

ⓢ Supporting Information

The Supporting Information is available free of charge at https://pubs.acs.org/doi/10.1021/acs.jpcc.3c00207.

> Sketch of the noise EC-STM working principle (Figure S1); Pt islands were deposited on a half Au/half Pd_{ML} on Au sample as sketched in the lower middle (Figure S2); polarization curve (cathodic sweep) of the Pt(111) sample (Figure S3); EC-STM data on Pt (111) for the ORR (Figure S4); schematic showing the junction comprised of two flat Pt electrodes and the scattering region used in electron tunneling calculations with the corresponding dimensions (Figure S5); left-hand side curve in each plot is the k-point averaged transmission spectrum as a function of energy (Figure S6); cut-plane representation of electron transmission eigenstates (Figure S7); computed tunneling current-voltage (Figure S8) (PDF)

■ AUTHOR INFORMATION

Corresponding Authors

Aliaksandr S. Bandarenka − *Physics of Energy Conversion and Storage, Department of Physics, Technical University of Munich, 85748 Garching bei München, Germany; Catalysis Research Center, Technical University of Munich, 85748 Garching bei München, Germany;* ⊙ orcid.org/0000-0002-5970-4315; Phone: +49 (89) 289-12531; Email: bandarenka@ph.tum.de; Fax: +49 (89) 289-12530

Vitaly Alexandrov − *Department of Chemical and Biomolecular Engineering, University of Nebraska-Lincoln, Lincoln, Nebraska 68588, United States;* ⊙ orcid.org/0000-0003-2063-6914; Phone: +1 (402) 472-5323; Email: valexandrov2@unl.edu; Fax: +1 (402) 472-6989

Authors

Mohammad R. Nouri − *Department of Chemical and Biomolecular Engineering, University of Nebraska-Lincoln, Lincoln, Nebraska 68588, United States*

Regina M. Kluge − *Physics of Energy Conversion and Storage, Department of Physics, Technical University of Munich, 85748 Garching bei München, Germany*

Richard W. Haid − *Physics of Energy Conversion and Storage, Department of Physics, Technical University of Munich, 85748 Garching bei München, Germany*

Jill Fortmann − *Materials Discovery and Interfaces, Institute for Materials, Ruhr University Bochum, D-44801 Bochum, Germany*

Alfred Ludwig − *Materials Discovery and Interfaces, Institute for Materials and Center for Interface-Dominated High Performance Materials, Ruhr University Bochum, D-44801 Bochum, Germany;* ⊙ orcid.org/0000-0003-2802-6774

Complete contact information is available at:
https://pubs.acs.org/10.1021/acs.jpcc.3c00207

Notes

The authors declare no competing financial interest.

■ REFERENCES

(1) Marcus, R. A. On the theory of oxidation-reduction reactions involving electron transfer. I. *J. Chem. Phys.* **1956**, *24*, 966−978.

(2) Marcus, R. A. On the theory of chemiluminescent electron-transfer reactions. *J. Chem. Phys.* **1965**, *43*, 2654−2657.

(3) Marcus, R. A. On the theory of electron-transfer reactions. VI. Unified treatment for homogeneous and electrode reactions. *J. Chem. Phys.* **1965**, *43*, 679−701.

(4) Hund, F. Zur deutung der molekelspektren. i. *Z. Phys.* **1927**, *40*, 742−764.

(5) Nordheim, L. Zur Theorie der thermischen Emission und der Reflexion von Elektronen an Metallen. *Z. Phys.* **1928**, *46*, 833−855.

(6) Gamow, G. Zur quantentheorie des atomkernes. *Z. Phys.* **1928**, *51*, 204−212.

(7) Merzbacher, E. The early history of quantum tunneling. *Phys. Today* **2002**, *55*, 44−49.

(8) Binnig, G.; Rohrer, H. Scanning tunneling microscopy. *Surf. Sci.* **1983**, *126*, 236−244.

(9) Binnig, G.; Rohrer, H. Scanning tunneling microscopy—from birth to adolescence. *Rev. Mod. Phys.* **1987**, *59*, 615.

(10) Zhuravlev, M. Y.; Sabirianov, R. F.; Jaswal, S.; Tsymbal, E. Y. Giant electroresistance in ferroelectric tunnel junctions. *Phys. Rev. Lett.* **2005**, *94*, No. 246802.

(11) Tsymbal, E. Y.; Kohlstedt, H. Tunneling across a ferroelectric. *Science* **2006**, *313*, 181−183.

(12) Zhu, J.-G. J.; Park, C. Magnetic tunnel junctions. *Mater. Today* **2006**, *9*, 36−45.

(13) Gajek, M.; Bibes, M.; Fusil, S.; Bouzehouane, K.; Fontcuberta, J.; Barthelemy, A.; Fert, A. Tunnel junctions with multiferroic barriers. *Nat. Mater.* **2007**, *6*, 296−302.

(14) Garcia, V.; Bibes, M. Ferroelectric tunnel junctions for information storage and processing. *Nat. Commun.* **2014**, *5*, 4289.

(15) Klyukin, K.; Tao, L.; Tsymbal, E. Y.; Alexandrov, V. Defect-assisted tunneling electroresistance in ferroelectric tunnel junctions. *Phys. Rev. Lett.* **2018**, *121*, No. 056601.

(16) Beratan, D. N.; Balabin, I. A. Heme−copper oxidases use tunneling pathways. *Proc. Natl. Acad. Sci. U. S. A.* **2008**, *105*, 403−404.

(17) Albrecht, T. Electrochemical tunnelling sensors and their potential applications. *Nat. Commun.* **2012**, *3*, 829.

(18) Fereiro, J. A.; Yu, X.; Pecht, I.; Sheves, M.; Cuevas, J. C.; Cahen, D. Tunneling explains efficient electron transport via protein junctions. *Proc. Natl. Acad. Sci. U. S. A.* **2018**, *115*, E4577−E4583.

(19) Gurney, R. The quantum mechanics of electrolysis. *Proc. R. Soc. London, Ser. A* **1931**, *134*, 137−154.

(20) Kuznetsov, A. M.; Sommer-Larsen, P.; Ulstrup, J. Resonance and environmental fluctuation effects in STM currents through large adsorbed molecules. *Surf. Sci.* **1992**, *275*, 52−64.

(21) Andersen, J. E.; Kornyshev, A. A.; Kuznetsov, A. M.; Madsen, L. L.; Møller, P.; Ulstrup, J. Electron tunnelling in electrochemical processes and in situ scanning tunnel microscopy of structurally organized systems. *Electrochim. Acta* **1997**, *42*, 819−831.

(22) Peskin, U.; Edlund, Å.; Bar-On, I.; Galperin, M.; Nitzan, A. Transient resonance structures in electron tunneling through water. *J. Chem. Phys.* **1999**, *111*, 7558−7566.

(23) Galperin, M.; Nitzan, A.; Benjamin, I. Numerical simulations of electron tunneling currents in water. *J. Phys. Chem. A* **2002**, *106*, 10790−10796.

(24) Simeone, F. C.; Kolb, D. M.; Venkatachalam, S.; Jacob, T. Tunneling behavior of electrified interfaces. *Surf. Sci.* **2008**, *602*, 1401−1407.

(25) Negre, C. F.; Jara, G. E.; Vera, D. M. A.; Pierini, A. B.; Sánchez, C. G. Detailed analysis of water structure in a solvent mediated electron tunneling mechanism. *J. Phys.: Condens. Matter* **2011**, *23*, No. 245305.

(26) Pan, J.; Jing, T.; Lindsay, S. Tunneling barriers in electrochemical scanning tunneling microscopy. *J. Phys. Chem.* **1994**, *98*, 4205−4208.

(27) Hugelmann, M.; Schindler, W. Tunnel barrier height oscillations at the solid/liquid interface. *Surf. Sci.* **2003**, *541*, L643−L648.

(28) Pfisterer, J. H.; Liang, Y.; Schneider, O.; Bandarenka, A. S. Direct instrumental identification of catalytically active surface sites. *Nature* **2017**, *549*, 74−77.

(29) Lunardon, M.; Kosmala, T.; Durante, C.; Agnoli, S.; Granozzi, G. Atom-by-atom identification of catalytic active sites in operando conditions by quantitative noise detection. *Joule* **2022**, *6*, 617−635.

(30) Mitterreiter, E.; Liang, Y.; Golibrzuch, M.; McLaughlin, D.; Csoklich, C.; Bartl, J. D.; Holleitner, A.; Wurstbauer, U.; Bandarenka,

A. S. In-situ visualization of hydrogen evolution sites on helium ion treated molybdenum dichalcogenides under reaction conditions. *npj 2D Mater. Appl.* **2019**, *3*, 1−9.

(31) Kosmala, T.; Baby, A.; Lunardon, M.; Perilli, D.; Liu, H.; Durante, C.; Di Valentin, C.; Agnoli, S.; Granozzi, G. Operando visualization of the hydrogen evolution reaction with atomic-scale precision at different metal−graphene interfaces. *Nat. Catal.* **2021**, *4*, 850−859.

(32) Liang, Y.; McLaughlin, D.; Csoklich, C.; Schneider, O.; Bandarenka, A. S. The nature of active centers catalyzing oxygen electro-reduction at platinum surfaces in alkaline media. *Energy Environ. Sci.* **2019**, *12*, 351−357.

(33) Haid, R. W.; Kluge, R. M.; Liang, Y.; Bandarenka, A. S. In situ quantification of the local electrocatalytic activity via electrochemical scanning tunneling microscopy. *Small Methods* **2021**, *5*, No. 2000710.

(34) Kluge, R. M.; Haid, R. W.; Bandarenka, A. S. Assessment of active areas for the oxygen evolution reaction on an amorphous iridium oxide surface. *J. Catal.* **2021**, *396*, 14−22.

(35) Nagy, G.; Wandlowski, T. Double layer properties of Au (111)/H2SO4 (Cl)+ Cu2+ from distance tunneling spectroscopy. *Langmuir* **2003**, *19*, 10271−10280.

(36) Kobayashi, Y.; Yokota, Y.; Wong, R. A.; Hong, M.; Takeya, J.; Osawa, S.; Ishiwari, F.; Shoji, Y.; Harimoto, T.; Sugimoto, K. Single-Molecule Observation of Redox Reactions Enabled by Rigid and Isolated Tripodal Molecules. *J. Phys. Chem. C* **2023**, *127*, 746−748.

(37) Smidstrup, S.; Markussen, T.; Vancraeyveld, P.; Wellendorff, J.; Schneider, J.; Gunst, T.; Verstichel, B.; Stradi, D.; Khomyakov, P. A.; Vej-Hansen, U. G. QuantumATK: an integrated platform of electronic and atomic-scale modelling tools. *J. Phys.: Condens. Matter* **2019**, *32*, No. 015901.

(38) Haid, R. W.; Kluge, R. M.; Schmidt, T. O.; Bandarenka, A. S. In-situ detection of active sites for carbon-based bifunctional oxygen reduction and evolution catalysis. *Electrochim. Acta* **2021**, *382*, No. 138285.

(39) Kluge, R. M.; Psaltis, E.; Haid, R. W.; Hou, S.; Schmidt, T. O.; Schneider, O.; Garlyyev, B.; Calle-Vallejo, F.; Bandarenka, A. S. Revealing the Nature of Active Sites on Pt−Gd and Pt−Pr Alloys during the Oxygen Reduction Reaction. *ACS Appl. Mater. Interfaces* **2022**, *14*, 19604−19613.

(40) Löffler, T.; Ludwig, A.; Rossmeisl, J.; Schuhmann, W. What Makes High-Entropy Alloys Exceptional Electrocatalysts? *Angew. Chem., Int. Ed.* **2021**, *60*, 26894−26903.

(41) Banko, L.; Krysiak, O. A.; Pedersen, J. K.; Xiao, B.; Savan, A.; Löffler, T.; Baha, S.; Rossmeisl, J.; Schuhmann, W.; Ludwig, A. Unravelling Composition−Activity−Stability Trends in High Entropy Alloy Electrocatalysts by Using a Data-Guided Combinatorial Synthesis Strategy and Computational Modeling. *Adv. Energy Mater.* **2022**, *12*, No. 2103312.

(42) Löffler, T.; Meyer, H.; Savan, A.; Wilde, P.; Garzón Manjón, A.; Chen, Y. T.; Ventosa, E.; Scheu, C.; Ludwig, A.; Schuhmann, W. Discovery of a multinary noble metal−free oxygen reduction catalyst. *Adv. Energy Mater.* **2018**, *8*, No. 1802269.